Chemical Science

ROYAL SOCIETY OF CHEMISTRY

EDGE ARTICLE

View Article Online
View Journal | View Issue

Cite this: *Chem. Sci.*, 2026, **17**, 2356

All publication charges for this article have been paid for by the Royal Society of Chemistry

Received 5th September 2025
Accepted 27th November 2025

DOI: 10.1039/d5sc06853c

rsc.li/chemical-science

Enantioselective synthesis of vicinal amino alcohols promoted by fluorine-containing counteranions

Yuchen Yang,[a] Jia-Long Wu,[a] Sheng-Ye Zhang,[b] Xu Liu,[a] Teng Sun,[a] Yanan Zhao *[b] and Lijia Wang *[a]

Chiral vicinal amino alcohols are pivotal building blocks in organic synthesis and pharmaceutical research. Herein, we report a chiral copper-catalyzed two-step one-pot strategy for the efficient synthesis of diaryl chiral vicinal amino alcohols, featuring excellent diastereoselectivity (>99 : 1 dr) and enantioselectivity (up to 99.5% ee). A key discovery is the critical role of fluorinated counteranions, which significantly enhance both reactivity and stereocontrol—an underappreciated effect in copper-catalyzed asymmetric reactions. DFT calculations reveal that secondary Cu–F interactions, combined with the spatial confinement of hexafluorophosphate, fine-tune the catalytic chiral environment, enabling precise stereocontrol *via* modulation of π–π stacking and weak non-covalent interactions. This strategy exhibits broad substrate scope, accommodating diverse aryl, heteroaryl, and functionalized substituents, and allows gram-scale synthesis with facile deprotection to free amino alcohols. The mechanistic insights into counterion effects highlight counterion engineering as a powerful tool for optimizing asymmetric catalysis.

Introduction

Chiral vicinal amino alcohols, endowed with unique structural and chiral features, occupy an irreplaceable pivotal position in organic synthesis, pharmaceutical research, chirotechnology, and materials science as key functional molecules bridging chemistry, biology, and materials science.[1] Since Kumada and co-workers first reported the asymmetric hydrogenation of amino ketones in 1979,[2] researchers have successively developed a variety of elaborate asymmetric catalytic strategies for the synthesis of chiral vicinal amino alcohols.[3] Among these, Sharpless asymmetric aminohydroxylation stands out as a landmark contribution, as it enables the direct, highly enantioselective construction of vicinal amino alcohol moieties from simple alkenes, revolutionizing the efficient and stereocontrolled synthesis of this important class of compounds.[4] However, the synthesis of chiral vicinal amino alcohols is constrained by several factors, including the scope of applicable substrates, functional group compatibility, and the simplicity of reaction conditions. Meanwhile, there is a growing demand for diverse chiral vicinal amino alcohols. As a result, new synthetic methods continue to emerge.[5–8] This highlights the critical need to develop novel asymmetric catalytic strategies that should be able to expand the structural diversity of chiral vicinal amino alcohols while enhancing their synthetic efficiency and accessibility.

The strategy of synthesizing chiral vicinal amino alcohols *via* nucleophilic asymmetric ring opening of epoxides or aziridines with nitrogen or oxygen nucleophiles represents one of the most straightforward and atom-economical approaches. Among these strategies, a powerful one is the desymmetrization of *meso*-substrates, as depicted in Fig. 1a. Pioneering work in this area was reported by Jacobsen and coworkers in 1998, who described the first chromium-catalyzed enantioselective nitrogen-nucleophilic ring opening of *meso*-epoxides.[9] Subsequently, Schneider *et al.*[10] and Feng *et al.*[11] independently developed asymmetric nitrogen-nucleophilic ring opening of *meso*-epoxides using chiral scandium(III) and indium(III) complexes, respectively. Alternatively, Toste *et al.*[12] and List *et al.*[13] utilized chiral phosphoric acid (CPA) catalysts to achieve the synthesis of chiral vicinal amino alcohols *via* alcohol-nucleophilic ring opening of *meso*-aziridiniums and *meso*-aziridines, respectively. More recently, Feng *et al.*[14] and Wang *et al.*[15] disclosed the oxygen-nucleophilic ring opening of *meso*-aziridines catalyzed by chiral magnesium complexes, further expanding the scope of this desymmetrization strategy. A complementary approach involves the kinetic resolution of racemic unsymmetric epoxides or aziridines (Fig. 1b). For example, Yamamoto and co-workers developed a chiral tungsten-catalyzed kinetic resolution of racemic 2,3-epoxy alcohols with aromatic amines for the construction of chiral vicinal amino alcohols.[16] In a related study, Cao *et al.* reported an efficient chiral phosphoric acid-catalyzed water-nucleophilic ring opening of racemic aziridines, which also proceeds *via*

[a]*Shanghai Engineering Research Center of Molecular Therapeutics and New Drug Development, Shanghai Frontiers Science Center of Molecule Intelligent Syntheses, East China Normal University, 3663 North Zhongshan Road, Shanghai 200062, China. E-mail: ljwang@chem.ecnu.edu.cn*

[b]*State Key Laboratory of Organometallic Chemistry, Shanghai Institute of Organic Chemistry, Chinese Academy of Sciences, 345 Lingling Lu, Shanghai 200032, China*

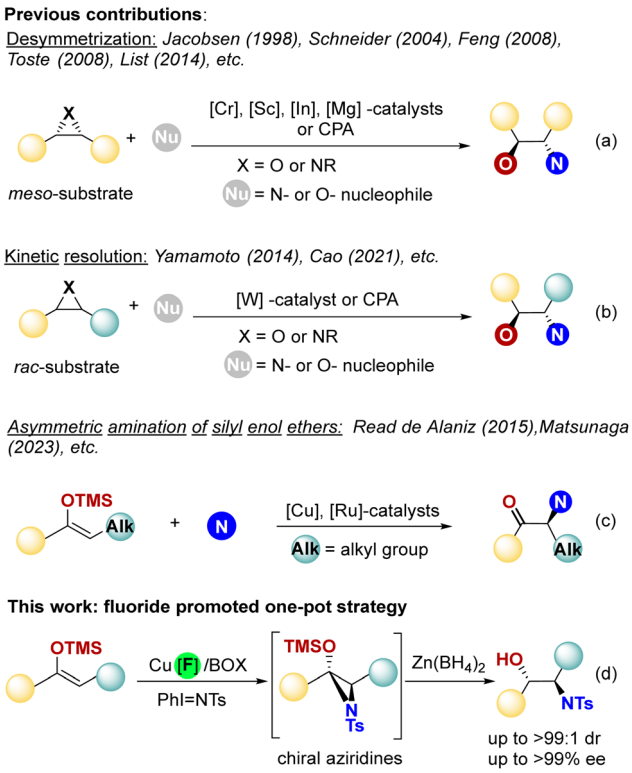

Fig. 1 Synthesis of chiral vicinal amino alcohols *via* asymmetric ring-opening of epoxides/aziridines.

a kinetic resolution pathway.[17] Although the aforementioned strategies for synthesizing chiral vicinal amino alcohols are direct and efficient, they suffer from limitations: being restricted to desymmetrization of *meso*-type substrates and, for unsymmetric substrates, requiring more than 2 equivalents of racemic starting materials to proceed *via* kinetic resolution.

In 1991, Evans and co-workers first discovered the Cu(I)-catalyzed amination of trimethylsilyl enol ethers to afford *N*-Ts amino ketones, postulating that the reaction proceeds *via* an aziridine ring-opening rearrangement pathway analogous to Rubottom oxidation.[18] This pioneering work initiated research into the asymmetric catalysis of this reaction.[19] In 2018, Read de Alaniz *et al.* developed a highly efficient Cu(I)-catalyzed asymmetric electrophilic α-amination of silyl enol ether derivatives *via* the nitrosocarbonyl hetero-ene reaction (Fig. 1c)[20] More recently, a landmark study by Matsunaga and colleagues demonstrated the chiral ruthenium-catalyzed amination of alkyl silyl enol ethers (Fig. 1c).[19f] However, no successful examples have been reported for diaryl-substituted silyl enol ether substrates. We conceived that developing a strategy involving asymmetric aziridination of silyl enol ethers with metal nitrenes,[21] combined with one-pot stereoselective reduction, could provide an alternative and efficient pathway for the synthesis of chiral diaryl vicinal amino alcohols (Fig. 1d). Although the hexafluorophosphate anion (PF_6^-) is widely employed as a counterion in copper-catalyzed asymmetric reactions, its role in asymmetric catalytic processes has long been overlooked.[22] This is likely due to the fact that PF_6^- is typically classified as a weakly coordinating anion (WCA) and was specifically designed to minimize interference with catalytic processes. Herein, we found that fluoro-containing counteranions can promote both the reactivity and enantioselectivity of the reaction. DFT calculations revealed that the interaction between a fluorine atom and the central copper metal can fine-tune the chiral environment of the catalytic center, thereby enabling the chiral copper-catalyzed one-pot synthesis of a series of diaryl chiral vicinal amino alcohols with excellent diastereo- and enantioselectivity.

Results and discussion

Initially, we investigated the reaction of the sterically hindered polysubstituted silyl enol ether **1a** with nitrene precursor **2** under catalysis by various chiral copper salts, followed by a one-pot reduction with zinc borohydride to directly afford the *N*-Ts protected chiral amino alcohol (Table 1, entries 1–9). When

Table 1 Optimization of the reaction[a]

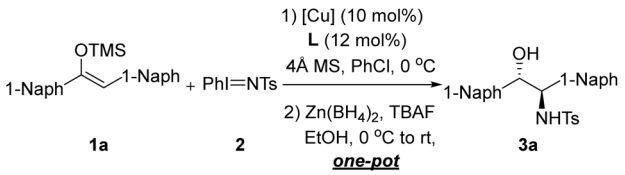

Entry	[Cu]	L	Yield[b] (%)	ee[c] (%)	dr[d]
1	$CuSO_4$	**L1**	N.D.	—	—
2	$Cu_3(PO_4)_2$	**L1**	N.D.	—	—
3	CuCN	**L1**	Trace	59	—
4	CuDPP	**L1**	Trace	68	—
5	CuTC	**L1**	Trace	76	—
6	$CuBr \cdot SMe_2$	**L1**	Trace	49	—
7	$Cu(ClO_4)_2 \cdot 6H_2O$	**L1**	32	75	96 : 4
8	$Cu(OTf)_2$	**L1**	26	77	90 : 10
9	CuOTf	**L1**	44	86	96 : 4
10	$Cu(CH_3CN)_4BF_4$	**L1**	34	88	94 : 6
11	$Cu(CH_3CN)_4PF_6$	**L1**	87	96	97 : 3
12	Cu(BArF)	**L1**	59	76	97 : 3
13	$Cu(CH_3CN)_4PF_6$	**L2**	34	71	93 : 7
14	$Cu(CH_3CN)_4PF_6$	**L3**	55	78	96 : 4
15	$Cu(CH_3CN)_4PF_6$	**L4**	51	78	94 : 6
16	$Cu(CH_3CN)_4PF_6$	**L5**	32	70	96 4
17[e]	$Cu(CH_3CN)_4PF_6$	**L1**	80	97	97 : 3

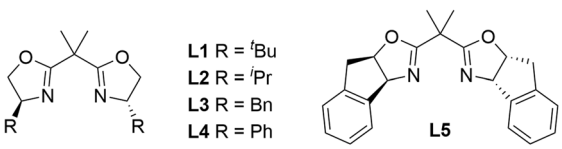

[a] Unless otherwise noted, all reactions were carried out with **1a** (0.2 mmol), **2** (0.3 mmol), 4 Å MS (100 mg), and Cu salt/**L** (1 : 1.2, 10 mol%) in PhCl (2.0 mL) under a N_2 atmosphere at 0 °C for 24 h, and then with $Zn(BH_4)_2$ (1.0 mmol, 1.0 M in THF), TBAF (0.6 mmol, 1.0 M in THF) and EtOH (1.0 mL) at 0 °C to rt for 4 h. [b] Isolated yield. [c] Determined by chiral HPLC. [d] Determined by crude ^1H NMR. [e] $LiAlH_4$ (1.0 mmol) was used instead of $Zn(BH_4)_2$.

copper sulfate and copper phosphate were employed, no desired product was detected (entries 1–2). In the case of cuprous cyanide, copper diphenylphosphinate (CuDPP), copper 2-thiophenecarboxylate (CuTC) and $CuBr\cdot SMe_2$, only trace amounts (<5% yield isolated by column chromatography) of the desired products were observed (entries 3–6). $Cu(ClO_4)_2\cdot 6H_2O$ could lead to 32% yield with 75% ee and a 96 : 4 dr (entry 7). Notably, during this process, we observed that the introduction of fluorine atoms into the counteranion significantly enhanced both the yield and enantioselectivity of the reaction. Using copper trifluoromethanesulfonate, the desired product **3a** was afforded in 26% yield with 77% ee and a 90 : 10 dr (entry 8). In contrast, cuprous trifluoromethanesulfonate improved the yield of **3a** to 44% with enhanced stereoselectivity (86% ee and 96 : 4 dr, entry 9). We further explored other fluorine-containing counteranions. The use of $Cu(CH_3CN)_4BF_4$ led to a slight improvement in enantioselectivity to 88% ee (entry 10), while $Cu(CH_3CN)_4PF_6$ resulted in further enhancements in both the yield and ee value, affording **3a** in 87% yield with 96% ee and a 97 : 3 dr (entry 11). To further verify the influence of fluorine atoms on the catalytic center, we tested the counteranion $BArF^-$, which might be spatially remote from the reaction center, and observed a significant decrease in both the yield and enantioselectivity of **3a** (59% yield and 76% ee, entry 12). Subsequently, we examined the effect of the chiral backbone of the ligands on the reaction and found that, among the chiral bisoxazoline (BOX) ligands tested, the one with a *tert*-butyl backbone (**L1**) outperformed those with other chiral backbones, such as isopropyl, benzyl, phenyl, and indenyl (**L2–L5,** entries 13–16). Thus, we identified $Cu(CH_3CN)_4PF_6$ as the optimal copper salt and **L1** as the optimal chiral ligand. Notably, we also investigated the effects of different reducing agents on the diastereoselectivity of the product. Although a 97 : 3 dr can also be achieved when $LiAlH_4$ is used as the reducing agent (entry 17), subsequent studies revealed that the diastereoselectivity of the reaction proved to be unsatisfactory when this reducing agent is applied to substrates with other substituents. Optimization of other reaction conditions can be found in the SI.

This one-pot strategy for the synthesis of chiral amino alcohols exhibits good substrate adaptability. Under the optimized reaction conditions (Table 1, entry 8), we explored structurally diverse diaryl-substituted enol silyl ethers (Table 2). When R^1 is 1-naphthyl and R^2 is 2-naphthyl, the corresponding amino alcohol **3b** was obtained in 93% yield with a 96 : 4 dr and 97% ee. Replacing the 2-naphthyl group with 5-benzofuranyl, 5-benzothienyl, or 5-benzodihydrofuranyl resulted in negligible changes in enantioselectivity, and the corresponding amino alcohols **3c–3e** were still afforded with 97–98% ee. Substrates **1f** and **1g** bearing more complex 3-fluorenyl and 2-dibenzofuranyl substituents were also compatible with this reaction, achieving 97% ee and 96% ee, respectively. When R^2 is a simple phenyl group, **3h** was obtained in 96% yield with a 98 : 2 dr and 98% ee. For substrate **1h**, we investigated the effect of different reducing agents on diastereoselectivity. $NaBH_4$ only resulted in diminished diastereoselectivity (74 : 26 dr), which is presumably due to the fact that zinc metal might be more ready to form chelating interactions with the substrate, which facilitates the control of diastereoselectivity during the reduction process. Interestingly, an inversion of diastereoselectivity (20 : 80 dr) can be achieved when DIBAL-H is used instead of $Zn(BH_4)_2$. Detailed results are available in the SI. Introduction of halogen substituents at different positions of the benzene ring (including fluorine, chlorine, and bromine) enabled the synthesis of the corresponding chiral amino alcohols **3i–3n** with 94–99% yields, 96 : 4 to >99 : 1 dr, and 93–96% ee. Incorporation of electron-withdrawing trifluoromethyl groups at the *para*- and *meta*-positions of the benzene ring led to a slight decrease in yield and enantioselectivity, giving **3o** and **3p** in 72% yield with 92% ee and 85% yield with 90% ee, respectively. Introduction of methyl groups at the *ortho*-, *para*-, and *meta*-positions of the benzene ring had almost no impact on the enantioselectivity of the reaction, and **3q–3s** were obtained with 97–98% ee. Although the introduction of an electron-rich methoxy group at the *ortho*-position of the benzene ring caused a decrease in enantioselectivity (**3t**, 90% ee), the corresponding product was obtained with exclusive enantioselectivity when the methoxy group was introduced at the *meta*-position (**3u**, 99.5% ee). For the *para*-methoxy-substituted substrate (**3v**), the reaction activity decreased slightly (84% yield), while the diastereoselectivity remained exclusive (>99 : 1 dr) and the enantioselectivity showed no significant change (97% ee). Other substituents on the benzene ring were also well-tolerated. For example, the 3,4-dimethoxy-substituted product **3w** was obtained in 73% yield with a 93 : 7 dr and 95% ee; the *para*-trifluoromethoxy-substituted substrate afforded the corresponding amino alcohol **3x** in 67% yield with a 98 : 2 dr and 92% ee. Reactive functional groups such as carboxyl, protected alcohol and amine derivatives were tolerated, affording **3y–3aa** with 90–95% ee. Bpin- and TMS-substituted substrates were also explored to give the corresponding **3bb** and **3cc** with 97–99% ee. Introduction of phenyl groups at the *ortho*-, *meta*-, and *para*- positions of the benzene ring led to the corresponding biphenyl amino alcohols **3dd–3ff** with 93–95% ee. When the phenyl group was replaced with a heteroaromatic ring, the reaction system remained compatible, and the thiophene-substituted amino alcohol **3gg** was synthesized in 96% yield with a 97 : 3 dr and 97% ee. The *tert*-butyl-aryl silyl enol ether was tried as substrate, and the desired product **3hh** could be obtained in 91% ee and >99 : 1 dr with 31% yield.

On the other hand, the Ar^1 group can also be extended in a variety of ways. For instance, naphthyl substrates substituted with fluorine, chlorine, or bromine atoms afforded the corresponding amino alcohols **3ii–3kk** in 96–99% yields with excellent diastereoselectivity and 97% ee. Naphthyl substrates with electron-donating substituents also performed well, giving **3ll** and **3mm** with 97–98% ee. Other more complex substituents were well compatible with the reaction, and the dibenzofuranyl-substituted product **3nn** was obtained with 94% ee. This method also allowed for the convenient preparation of various dimethyl-substituted phenyl amino alcohols **3oo–3qq** as well as 1,2-diaryl-substituted amino alcohol **3rr** with 95–97% ee. Meanwhile, the absolute configuration of product **3a** was confirmed to be (1*R*, 2*S*) by X-ray diffraction analysis of its single crystal.

Table 2 Substate scope[a]

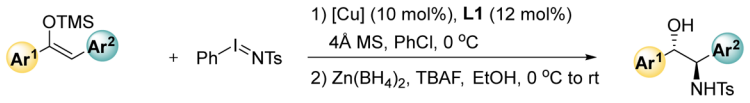

1 2 3

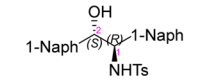

3a
87%, 97:3 dr, 96% ee

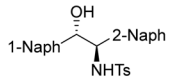

3b
93%, 96:4 dr, 97% ee

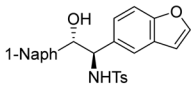

3c
55%, 99:1 dr, 97% ee

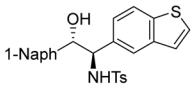

3d
80%, 96:4 dr, 98% ee

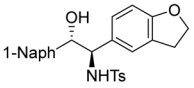

3e
62%, 96:4 dr, 97% ee

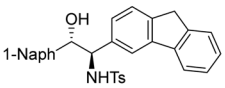

3f
61% yield, 92:8 dr, 97% ee

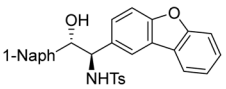

3g
99%, >99:1 dr, 96% ee

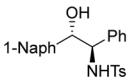

3h
96%, 98:2 dr, 98% ee

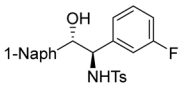

3i
97% yield, 96:4 dr, 96% ee

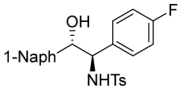

3j
98%, >99:1 dr, 95% ee

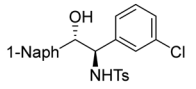

3k
95%, 96:4 dr, 96% ee

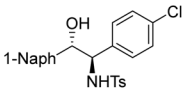

3l
99% yield, >99:1 dr, 93% ee

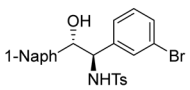

3m
94%, 99:1 dr, 96% ee

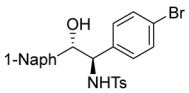

3n
96%, 97:3 dr, 95% ee

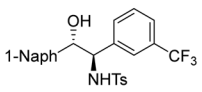

3o[b]
72% yield, 95:5 dr, 92% ee

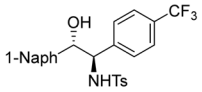

3p
85%, 98:2 dr, 90% ee

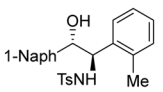

3q
91% , >99:1 dr, 98% ee

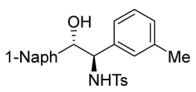

3r
95%, 99:1dr, 97% ee

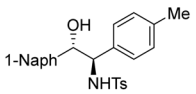

3s
83%, 96:4 dr, 98% ee

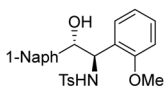

3t
95% yield, 98:2 dr, 90% ee

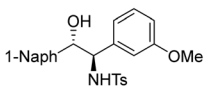

3u
90% yield, 97:3 dr, 99.5 % ee

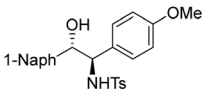

3v
84%, >99:1 dr, 97% ee

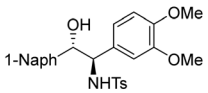

3w
73%, 93:7 dr, 95% ee

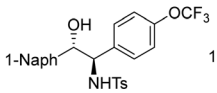

3x
67%, 98:2 dr, 92% ee

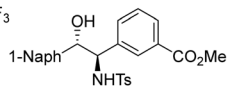

3y
73% yield, 96:4 dr, 95 % ee

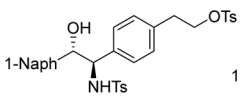

3z
51%, 97:3 dr, 93% ee

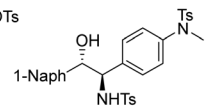

3aa[b]
73%, 96:4 dr, 90% ee

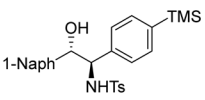

3bb
88%, 96:4 dr, 97% ee

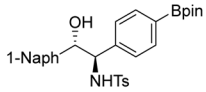

3cc
85%, 97:3 dr, 99% ee

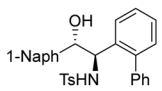

3dd
84%, 98:2 dr, 93% ee

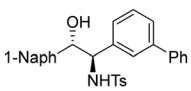

3ee
95%, 97:3 dr, 95% ee

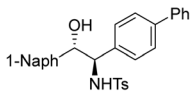

3ff
99%, 97:3 dr, 95% ee

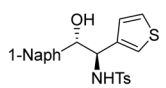

3gg
96%, 97:3 dr, 97% ee

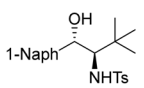

3hh[c]
31%, >99:1 dr, 91% ee

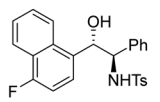

3ii
96%, 98:2 dr, 97% ee

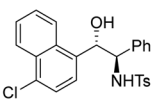

3jj
96%, 97:3 dr, 97% ee

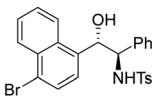

3kk
99%, 96:4 dr, 97% ee

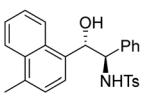

3ll
74%, 97:3 dr, 98% ee

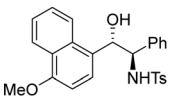

3mm
85%, 97:3 dr, 97% ee

3nn
83%, 97:3 dr, 94% ee

3oo
84%, >99:1 dr, 97% ee

3pp
76%, >99:1 dr, 97% ee

3qq
62%, >99:1 dr, 97% ee

3rr
86%, >99:1 dr, 95% ee

3a

[a] Unless otherwise noted, all reactions were carried out with **1** (0.2 mmol), **2** (0.3 mmol), 4 Å MS (100 mg), and $Cu(CH_3CN)_4PF_6$/**L1** (1 : 1.2, 10 mol%) in PhCl (2.0 mL) under a N_2 atmosphere at 0 °C for 24 h, and then $Zn(BH_4)_2$ (1.0 mmol, 1.0 M in THF), TBAF (0.6 mmol, 1.0 M in THF) and EtOH (1.0 mL) were added at 0 °C to rt for 4 h; Isolated yield; dr value was determined by crude ^1H NMR; ee value was determined by chiral HPLC. [b] −10 °C. [c] **2** was added in four portions.

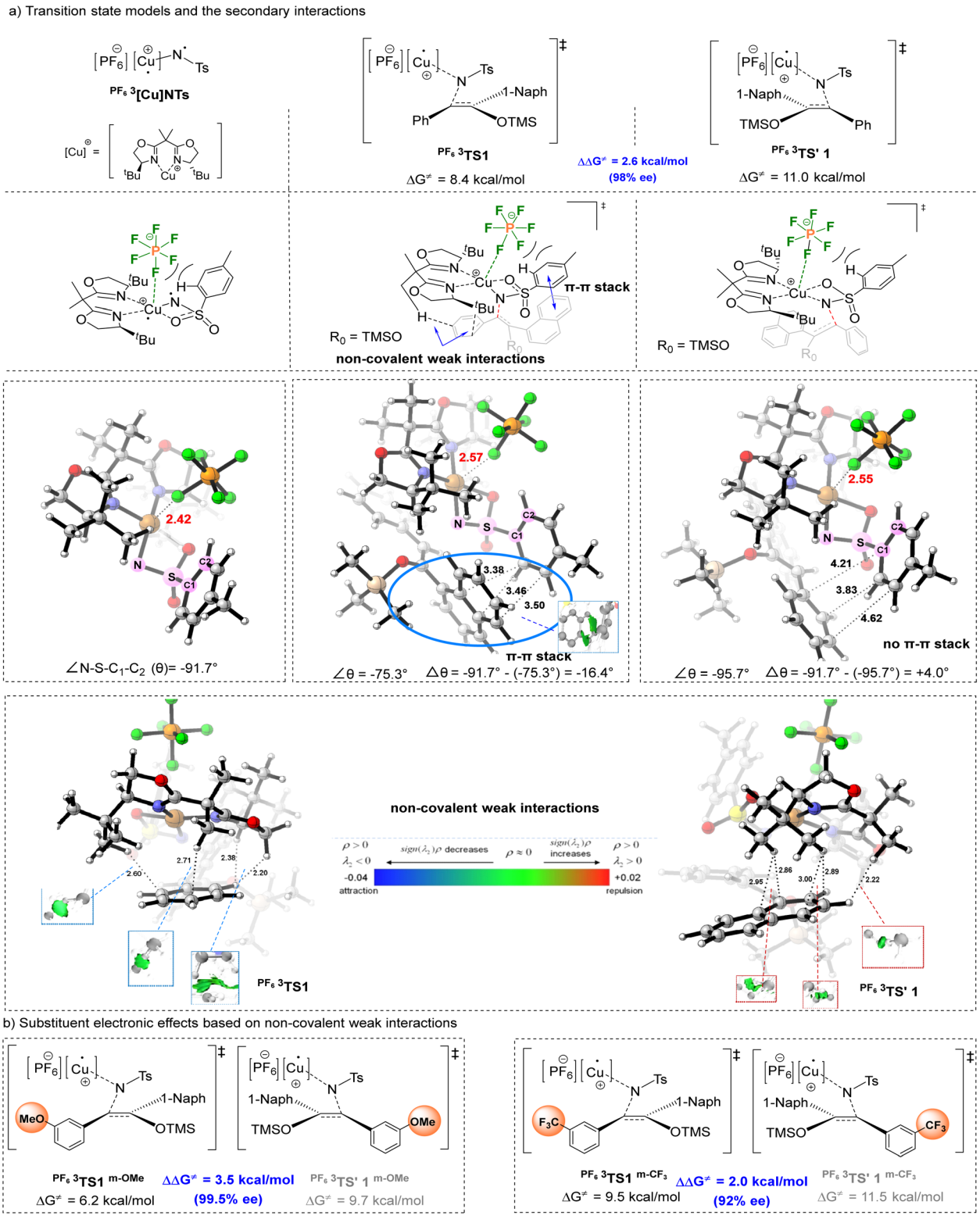

Fig. 2 DFT-derived interactions in the enantioselective induction model.

To gain insights into the fluoride benefited reaction mechanism, density functional theory (DFT) calculations were performed on the pathway of the asymmetric aziridination reaction between copper nitrenes and silyl enol ethers, based on the reported computational literature studies (calculation details and the reaction potential energy surface calculations are provided in the SI).[23] DFT calculations revealed that the initiating species of the reaction is ^{PF_6} ^{3}[Cu]NTs, corresponding to

the structure where the triplet nitrene and ligand are coordinated to Cu^{+}, respectively. During the reaction, for the major and minor enantiomers, the rate-determining step involves the formation of the first N–C bond *via* the transition states (TS) with the highest energy barrier, ^{PF_6}**^{3}TS1** ($\Delta G^{\neq} = 8.4$ kcal mol^{-1}) and ^{PF_6}**^{3}TS'1** ($\Delta G^{\neq} = 11.0$ kcal mol^{-1}), which thus serves as the chirality determining step. The calculated $\Delta\Delta G^{\neq}$ for this step is 2.6 kcal mol^{-1}, consistent with the experimental 98% ee (Fig. 2a).

Notably, calculations indicated that in the initiating species ^{PF_6}**^{3}[Cu]NTs**, one of the F atoms of the anion exhibit certain coordination interactions with Cu, with a Cu–F distance of 2.42 Å (significantly shorter than the sum of the van der Waals radii of Cu and F, 2.87 Å). Such secondary interactions enable the hexafluorophosphate ion to occupy the space above the ^{PF_6}**^{3}[Cu]NTs** species, confining the Ts group to the region below the anion (Fig. 2a). The identification of these Cu–F secondary interactions corroborates the experimental observation that fluorinated counterions influence reaction activity and enantioselectivity. In the TS of the major enantiomer (^{PF_6}**^{3}TS1**), as the silyl enol ether substrate approaches the reaction center, the spatial confinement by the hexafluorophosphate ion induces a conformational change in the Ts group, facilitating its deformation and π–π stacking with the naphthyl ring of the silyl enol ether—this contributes to the lower energy of ^{PF_6}**^{3}TS1**. As shown in Fig. 2a, the dihedral angle ∠N–S–C1–C2 (θ) changes from −91.7° in ^{PF_6}**^{3}[Cu]NTs** to −75.3° in ^{PF_6}**^{3}TS1**, corresponding to a 16.4° rotation of the benzene ring in the Ts group around the S–C1 bond. In contrast, no such π–π stacking is observed in ^{PF_6}**^{3}TS'1**, and the variation in ∠θ is comparatively small.

The presence of the hexafluorophosphate ion also affects the conformation of the BOX ligand. IGMH (Independent Gradient Model based on Hirshfeld partition) analysis revealed two pairs of C···H weak interactions and two pairs of H···H weak attractive interactions between the benzene ring and the ligand in ^{PF_6}**^{3}TS1**, which favor its lower energy barrier. In contrast, the weak interactions between the naphthyl ring and the ligand in ^{PF_6}**^{3}TS'1** are less pronounced. Based on the above IGMH analysis, the weak interaction sites in ^{PF_6}**^{3}TS1** are located at the *ortho*- and *para*-positions of the phenyl substituent. Thus, introducing an electron-donating substituent (*e.g.*, methoxy) at the *meta*-position of the benzene ring is expected to enhance these electrostatic attractions, thereby lowering the energy barrier of ^{PF_6}**^{3}TS1** and increasing the energy barrier difference between ^{PF_6}**^{3}TS1** and ^{PF_6}**^{3}TS'1** (*i.e.*, enhancing the ee value). Calculations showed that the energy barrier difference increases from 2.6 kcal mol^{-1} to 3.5 kcal mol^{-1}, consistent with the experimental improvement in the ee value from 98% to 99.5% (Fig. 2b). Conversely, introducing an electron-withdrawing substituent (*e.g.*, trifluoromethyl) at this position might have the opposite effect: the calculated energy barrier difference decreased to 2.0 kcal mol^{-1}, and the experimental ee value dropped from 98% to 92% (Fig. 2b). These computational results are in good agreement with the experimental data, validating the reliability of the theoretical model.

This method provides a practical approach for the gram-scale synthesis of disubstituted chiral amino alcohols.

With 1,2-Dinaphthyl-substituted amino alcohol **3a**, 1,2-diaryl-substituted amino alcohol **3rr**, or the product **3h** with two different substituents, the reaction can be successfully scaled up to the gram level, affording 79–94% yield with 3.42 g to 3.92 g (Fig. 3). Moreover, the resulting products can be isolated and purified by recrystallization to afford optically pure products with >99% ee and >99 : 1 dr. It is worth noting that these *N*-Ts protected amino alcohols can undergo mild and convenient deprotection under Red-Al conditions, thereby yielding the corresponding optically pure chiral amino alcohols **4a**, **4rr**, and **4h** in 60–70% yields.

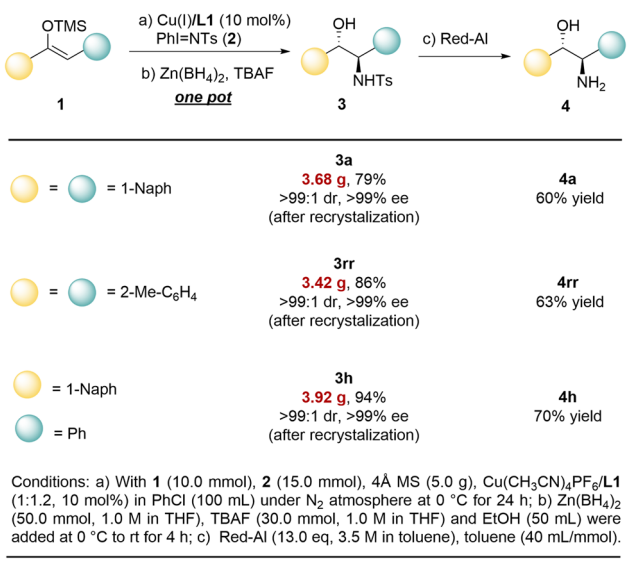

Fig. 3 Gram scale synthesis and transformation.

Conclusions

In summary, we report a chiral copper-catalyzed two-step one-pot strategy for the synthesis of diaryl chiral vicinal amino alcohols with excellent diastereo- and enantioselectivity (up to >99 : 1 dr and 99.5% ee). A key innovation is the identification of fluorinated counteranions as critical regulators of reactivity and enantioselectivity—an underappreciated role in copper catalysis. DFT calculations revealed that secondary Cu–F interactions, coupled with the spatial confinement of hexafluorophosphate, fine-tune the catalytic chiral environment to enable precise stereocontrol, as validated by IGMH analysis. This method features broad substrate scope, gram-scale accessibility, and facile deprotection to free amino alcohols, offering a robust platform for accessing valuable chiral vicinal amino alcohols. Importantly, it highlights counterion engineering as a powerful tool for optimizing asymmetric catalytic performance.

Author contributions

L. W. conceived and directed the project, and prepared the manuscript; Y. Y. performed all the experiments and the

experiment part of the SI; J.-L. W. performed the DFT calculation and the calculation part of the SI; S.-Y. Z. provided useful DFT calculation suggestions; Y. Z. supervised DFT calculations and the calculation part of the SI; X. L. and T. S. synthesized some substrates.

Conflicts of interest

The authors declare no competing financial interest.

Data availability

The data supporting this article have been included as part of the supplementary information (SI). Supplementary information is available. Supplementary information: experimental procedures, spectroscopic data for new compounds, NMR, HRMS spectra and HPLC chromatograms, and CIF file of enantiopure product **3a**. See DOI: https://doi.org/10.1039/d5sc06853c.

CCDC 2478618 (**3a**) contains the supplementary crystallographic data for this paper.[24]

Acknowledgements

This work was supported by the National Natural Science Foundation of China (91956103 and 22571088), the Science and Technology Commission of Shanghai Municipality (23JC1404500), the Strategic Priority Research Program of the Chinese Academy of Sciences (XDB0610000) and the Fundamental Research Funds for the Central Universities. We also thank Dr Xiao-Li Zhao for X-ray crystal analysis.

Notes and references

1 (*a*) P. Gupta, and N. Mahajan, in *Chemistry of Biologically Potent Natural Products and Synthetic Compounds*, ed. Shahid-ul-Islam and J. A. Banday, Scrivener Publishing LLC, 2021; (*b*) Y.-J. Cheng, L.-P. Zhao, L. Wang and Y. Tang, *CCS Chem.*, 2023, **5**, 124; (*c*) P.-J. Li, P.-C. Yin, L. Wang and Y. Tang, *CCS Chem.*, 2025, DOI: 10.31635/ccschem.025.202506445.

2 T. Hayashi, A. Katsumura, M. Konishi and M. Kumada, Asymmetric synthesis of 2-amino-1-arylethanols by catalytic asymmetric hydrogenation, *Tetrahedron Lett.*, 1979, **20**, 425–428.

3 (*a*) S. C. Bergmeier, *Tetrahedron*, 2000, **56**, 2561–2576; (*b*) T. J. Donohoe, C. K. A. Callens, A. Flores, A. R. Lacy and A. H. Rathi, *Chem.–Eur. J.*, 2011, **17**, 58–76; (*c*) B. N. Hemric, *Org. Biomol. Chem.*, 2021, **19**, 46–81; (*d*) X. Yan, W. Feng, J. X. Ng, J. Li, Y. Liu, B. Zhang, P.-L. Shao and Y. Zhao, *Chem. Soc. Rev.*, 2025, **54**, 7966–8018.

4 (*a*) G. Li, H.-T. Chang and K. B. Sharpless, *Angew. Chem., Int. Ed.*, 1996, **35**, 451–454; (*b*) P. O'Brien and K. B. Sharpless, *Angew. Chem., Int. Ed.*, 1999, **38**, 326–329.

5 For recent leading examples on asymmetric hydrogenation, see: (*a*) J. Wang, X. Lin, P.-L. Shao, J. Song, J. Wen and X. Zhang, *ACS Catal.*, 2021, **11**, 12729–12735; (*b*) Y. Xu, Y. Luo, J. Ye, Y. Deng, D. Liu and W. Zhang, *J. Am. Chem. Soc.*, 2022, **144**, 20078–20089; (*c*) M. Zhang, T. Niu, M. Liang, F. Xu, Y. Du, H. Zhuang, R.-J. Song, H. Yang and Q. Yin, *J. Am. Chem. Soc.*, 2025, **147**, 18197–18207.

6 For recent leading examples on asymmetric reductive coupling, see: (*a*) C.-X. Ye, Y. Y. Melcamu, H.-H. Li, J.-T. Cheng, T.-T. Zhang, Y.-P. Ruan, X. Zheng, X. Lu and P.-Q. Huang, *Nat. Commun.*, 2018, **9**, 410; (*b*) H. Hu and Z. Wang, *J. Am. Chem. Soc.*, 2023, **145**, 20775–20781; (*c*) T. Bender and A. Fürstner, *J. Am. Chem. Soc.*, 2024, **146**, 33295–33301; (*d*) Z. Chi, J.-B. Liao, X. Cheng, Z. Ye, W. Yuan, Y.-M. Lin and L. Gong, *J. Am. Chem. Soc.*, 2024, **146**, 10857–10867; (*e*) J. Zhu, F. Rahim, P. Zhou, A. Zhang and S. J. Malcolmson, *J. Am. Chem. Soc.*, 2024, **146**, 20270–20278.

7 For recent leading examples on asymmetric radical addition, see: (*a*) J. Caner, A. Matsumoto and K. Maruoka, *Chem. Sci.*, 2023, **14**, 13879–13884; (*b*) H. Hu, Z. Shi, X. Guo, F.-H. Zhang and Z. Wang, *J. Am. Chem. Soc.*, 2024, **146**, 5316–5323; (*c*) Z. Zhong, H. Wu, X. Chen, Y. Luo, L. Yang, X. Feng and X. Liu, *J. Am. Chem. Soc.*, 2024, **146**, 20401–20413.

8 For recent leading examples on miscellaneous strategies, see: (*a*) E. M. Mumford, B. N. Hemric and S. E. Denmark, *J. Am. Chem. Soc.*, 2021, **143**, 13408–13417; (*b*) C. Hou, B. Peng, S. Ye, Z. Yin, J. Cao, X. Xiao and B. Zhao, *Nat. Catal.*, 2022, **5**, 1061–1068; (*c*) B. G. Hejna, J. M. Ganley, H. Shao, H. Tian, J. D. Ellefsen, N. J. Fastuca, K. N. Houk, S. J. Miller and R. R. Knowles, *J. Am. Chem. Soc.*, 2023, **145**, 16118–16129; (*d*) H. Yan, Q. Liao, Y. Chen, G. G. Gurzadyan, B. Lu, C. Wu and L. Shi, *Angew. Chem., Int. Ed.*, 2023, **62**, e202302483; (*e*) A. Mondal and G. C. Fu, *J. Am. Chem. Soc.*, 2025, **147**, 10859–10863.

9 L. E. Martinez, J. L. Leighton, D. H. Carsten and E. N. Jacobsen, *J. Am. Chem. Soc.*, 1995, **117**, 5897–5898.

10 C. Schneider, A. R. Sreekanth and E. Mai, *Angew. Chem., Int. Ed.*, 2004, **43**, 5691–5694.

11 B. Gao, Y. Wen, Z. Yang, X. Huang, X. Liu and X. Feng, *Adv. Synth. Catal.*, 2008, **350**, 385–390.

12 G. L. Hamilton, T. Kanai and F. D. Toste, *J. Am. Chem. Soc.*, 2008, **130**, 14984–14986.

13 M. R. Monaco, B. Poladura, M. Diazde Los Bernardos, M. Leutzsch, R. Goddard and B. List, *Angew. Chem., Int. Ed.*, 2014, **53**, 7063–7067.

14 J. Li, Y. Liao, Y. Zhang, X. Liu, L. Lin and X. Feng, *Chem. Commun.*, 2014, **50**, 6672–6674.

15 L. Wang, D. Yang, D. Li, H. Zhu, P. Wang, X. Liu, L. Bai and R. Wang, *Adv. Synth. Catal.*, 2018, **360**, 4491–4496.

16 (*a*) C. Wang and H. Yamamoto, *Angew. Chem., Int. Ed.*, 2014, **53**, 13920–13923; (*b*) C. Wang and H. Yamamoto, *J. Am. Chem. Soc.*, 2015, **137**, 4308–4311.

17 J. Liu, Y.-Y. Du, Y.-S. He, Y. Liang, S.-Z. Liu, Y.-Y. Li and Y.-M. Cao, *Chem. Sci.*, 2023, **14**, 12152–12159.

18 D. A. Evans, M. M. Faul and M. T. Bilodeau, *J. Org. Chem.*, 1991, **56**, 6744–6746.

19 (*a*) W. Adam, K. J. Roschmann and C. R. Saha-Möller, *Eur. J. Org Chem.*, 2000, **2000**, 557–561; (*b*) J.-L. Liang, X.-Q. Yu and C.-M. Che, *Chem. Commun.*, 2002, 124–125; (*c*) M. Anada,

M. Tanaka, T. Washio, M. Yamawaki, T. Abe and S. Hashimoto, *Org. Lett.*, 2007, **9**, 4559–4562; (*d*) M. Tanaka, Y. Kurosaki, T. Washio, M. Anada and S. Hashimoto, *Tetrahedron Lett.*, 2007, **48**, 8799–8802; (*e*) M. Nakanishi, C. Minard, P. Retailleau, K. Cariou and R. H. Dodd, *Org. Lett.*, 2011, **13**, 5792–5795; (*f*) K. Makino, Y. Kumagai, T. Yoshino, M. Kojima and S. Matsunaga, *Org. Lett.*, 2023, **25**, 3234–3238.

20 D. Sandoval, A. V. Samoshin and J. Read de Alaniz, *Org. Lett.*, 2015, **17**, 4514–4517.

21 (*a*) B. Liu, P. Xie, J. Zhao, J. Wang, M. Wang, Y. Jiang, J. Chang and X. Li, *Angew. Chem., Int. Ed.*, 2021, **60**, 8396–8400; (*b*) R. Mi, Z. Ding, S. Yu, R. H. Crabtree and X. Li, *J. Am. Chem. Soc.*, 2023, **145**, 8150–8162; (*c*) N. J. Hodson, S. Takano, A. Fanourakis and R. J. Phipps, *J. Am. Chem. Soc.*, 2024, **146**, 22629–22641.

22 (*a*) C.-T. Li, L.-G. Liu, J.-Z. Li, H.-X. Dong, R. A. Novikov, Z.-S. Wang, X. Hong, B. Zhou and L.-W. Ye, *Nat. Commun.*, 2025, **16**, 4107; (*b*) S. Maurya, N. Navaneetha, P. Behera, J. B. Nanubolu, L. Roy and R. Chegondi, *Angew. Chem., Int. Ed.*, 2025, **64**, e202420106; (*c*) K. Morisaki, Y. Furuki, R. Kousaka, S. Nagai, Y. Oonishi and Y. Sato, *J. Am. Chem. Soc.*, 2025, **147**, 12740–12748; (*d*) C.-Y. Weng, L.-G. Liu, M. Sun, X. Lu, X. Hong, L.-W. Ye and B. Zhou, *Angew. Chem., Int. Ed.*, 2025, **64**, e202418254; (*e*) X. Zhang, Y. Zhou, Z.-X. Yu, C.-H. Tung and Z. Xu, *Angew. Chem., Int. Ed.*, 2025, **64**, e202420667.

23 (*a*) P. Brandt, M. J. Södergren, P. G. Andersson and P.-O. Norrby, *J. Am. Chem. Soc.*, 2000, **122**, 8013–8020; (*b*) L. Maestre, W. M. C. Sameera, M. M. Díaz-Requejo, F. Maseras and P. J. Pérez, *J. Am. Chem. Soc.*, 2013, **135**, 1338–1348; (*c*) M. R. Rodríguez, A. M Rodríguez, S. López-Resano, M. A. Pericàs, M. M. Díaz-Requejo, F. Maseras and P. J. Pérez, *ACS Catal.*, 2023, **13**, 706–713; (*d*) S.-Y. Zhang, Y. Zhao, L. Wang, Z.-P. Liu and Y. Tang, *CCS Chem.*, 2025, **7**, 3493–3506.

24 CCDC 2478618, (**3a**): Experimental Crystal Structure Determination, 2025, DOI: 10.5517/ccdc.csd.cc2p66fk.